 ©2015 Uspekhi Fizicheskikh Nauk, Russian Academy of Sciences

REVIEWS OF TOPICAL PROBLEMS PACS numbers: 42.79.Pw, 85.60.Gz

Photon far-infrared and submillimeter array detectors

I G Neizvestnyi, A E Klimov, V N Shumsky

DOI: 10.3367/UFNe.0185.201510b.1031

Contents

Abstract. This review analyzes the current state of research pertaining to the design of thermal and photon far-infrared and submillimeter array detectors. Threshold detector characteristics are compared and the application potential of photodetectors is explored.

Keywords: array photodetectors, infrared region, submillimeter-wave region, imaging

1. Introduction

The development of detectors for far-infrared (FIR) and submillimeter (SMM) radiation with wavelengths $\lambda = 0.03-0.3$ mm (for the terahertz frequency range with $f = 10^{-1}$ THz, respectively) has recently become topical in connection with the broadening of basic knowledge acquired in studies of SMM radiation interaction with different physical objects. In so doing, the scientific and practical problems which may be solved with the employment of these detectors are classed into two groups, depending on whether use is made of intrinsic thermal emission (passive operating mode) or radiation from an independent source reflected from an object (active mode).

A number of related problems, like, for instance, astrophysical research and circumterrestrial space monitoring, call not only for an extremely high threshold characteristic of individual photodetectors (PDs) owing to low thermal radiation fluxes, but also for the development of photodetector arrays (PDAs). The same requirements are imposed on PDA devices intended for imaging objects in the IR and SMM ranges with the use of only their intrinsic thermal radiation. Apart from increasing the signal-to-noise ratio, PDAs permit, in principle, either simplifying the scanning systems in such devices or completely abandoning them.

Meanwhile, the operation of active (with illumination) SMM devices intended, for instance, for security systems (detection of illicit enclosures and objects, including those on the human body) permits using other detectors as well. These include uncooled microbolometer PDAs with a rather high noise equivalent power (NEP), which is primarily related to the radiation source power. Such detectors are not discussed in our paper.

SMM radiation detectors have been described in several papers including reviews [1–4]. The purpose of our work is to analyze the parameters of thermal and photon detectors for the FIR and submillimeter regions, to compare their threshold characteristics, and also to consider the possibility of producing PDAs and estimating the prospects of their application.

2. Photodetectors with superconducting materials

Prior to describing the specific parameters of photodetectors, we recall their generally accepted definitions.

1. Ampere–watt (volt–watt) responsivity:

$$S_i = \frac{\mathrm{d}I}{\mathrm{d}P} \quad \left(S_v = \frac{\mathrm{d}V}{\mathrm{d}P}\right),$$

where I is the current, and V is the voltage seen by the external circuit of a PD exposed to radiation of power P. The responsivity is termed spectral when the radiation is monochromatic or integral when the radiation covers some spectral band.

2. Noise equivalent power is the power of the radiation flux which induces a signal at the photodetector output equal to the noise in a unit frequency band. The NEP dimensionality is W $\mathrm{Hz}^{-0.5}$.

3. Detectivity per Hz frequency band per cm^2:

$$D^* = \frac{S_i\sqrt{A\Delta f}}{i_\mathrm{n}},$$

I G Neizvestnyi, A E Klimov, V N Shumsky Rzhanov Institute of Semiconductor Physics,
Siberian Branch of the Russian Academy of Sciences,
prosp. Akademika Lavrentieva 13, 630090 Novosibirsk,
Russian Federation
E-mail: neizv@isp.nsc.ru, klimov@isp.nsc.ru, shumsky@isp.nsc.ru

Received 25 June 2015, revised 24 July 2015
Uspekhi Fizicheskikh Nauk **185** (10) 1031 – 1042 (2015)
DOI: 10.3367/UFNr.0185.201510b.1031
Translated by E N Ragozin; edited by A Radzig

where i_n is the root-mean-square noise level, A is the detector area, and Δf is the amplifier bandwidth. The unit of measurement of detectivity (Jones) has dimensionality cm $Hz^{0.5}$ W^{-1}.

Bolometers

Bolometers are traditional nonselective radiation detectors in which an absorption layer is heated under irradiation. The heating results in changes to the resistance of the active layer (thermometer), which is attended with changes in electric current in the circuit. High-sensitivity cooled bolometers are nowadays made on the basis of superconducting materials — so-called superconducting transition-edge sensors, or TES bolometers. In the vicinity of the transition point, the slope of curve is steep and the detector resistance greatly depends on the temperature, so the bolometer responsivity is high.

Simoens et al. [5] described a set of cooled bolometers intended for operation in a photometer and spectrometer of far-infrared and submillimeter (terahertz) radiation aboard the Herschel Space Observatory, which was developed under the auspices of the European Space Agency. The photometer consisted of two focal-plane arrays 32×64 and 16×32 pixels in size. The array for shorter-wavelength radiation (32×64) was intended for the 60–90 and 90–130 μm ranges, and the longer-wavelength array for 130–210 μm radiation. The photometer was cooled to $T = 0.3$ K. Preliminary test data suggested that the NEP level was about 10^{-16} W $Hz^{-0.5}$, which was close to the background-restricted limit.

Pajot et al. [6, 7] reported on the development of high-sensitivity bolometers based on thin (100 nm) films of a niobium–silicon (NbSi) alloy. The NbSi alloys may be semiconductors or superconductors, depending on the niobium concentration. For a niobium content of 13%, the semiconductor nature of the temperature dependence of the resistivity changes to that typical for superconductors. For the alloy composition investigated, the transition temperature was $T_C = 0.593$ K; the spread of this temperature for a 23-pixel array was within ±0.001 K. The noise was at a level of 1.8×10^{-11} A $Hz^{-0.5}$, and the NEP turned out to be equal to 1.35×10^{-16} W $Hz^{-0.5}$.

Rogalsky and Sizov [3] reported on the development of a focal plane array based on TES bolometers and intended for operation with the telescope of the Atacama (Space) Observatory in the 0.1–3.0 THz frequency band. They considered methods for optimizing the response time and sensitivity of the array made on a 4-inch (∼ 100 mm) silicon chip by introducing an AuPd alloy-based ohmic shunt to each TES element, which were made using molybdenum nitride (MoN_x).

Bintley et al. [8] reported, as a revolution in submillimeter astronomy, the development of an SMM camera with a 10^4-pixel matrix operating at wavelengths of 450 and 850 μm, which was intended for studying the nature of galaxies, stars, and planets with the Maxwell Telescope (Mauna Kea Observatory). The detector had presented itself a copper–molybdenum TES bolometer attached to a silicon nitride membrane and connected to a multiplexer plate via metallic columns. The detector structure is schematized in Fig. 1.

For a detector responsivity exceeding 10^6 A W^{-1}, the NEP was found to be equal to 1.12×10^{-16} W $Hz^{-0.5}$ at wavelength $\lambda = 450$ μm, and to 4.2×10^{-17} W $Hz^{-0.5}$ at wavelength $\lambda = 850$ μm. The transition temperature T_C was equal to 0.194 and 0.135 K, respectively.

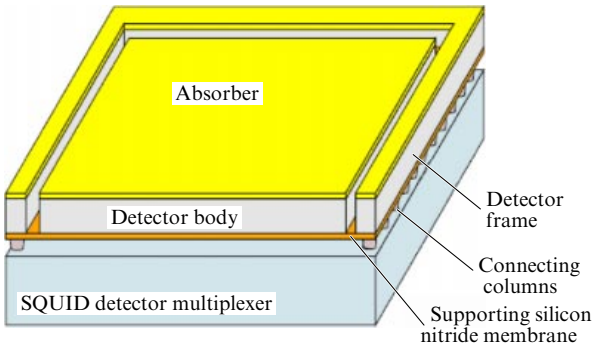

Figure 1. Schematic representation of a copper–molybdenum TES bolometer.

A special operation feature of bolometers at low temperatures is that electrons interact only slightly with phonons in a superconductor, and their temperature therefore becomes higher than the lattice temperature. Such bolometers are referred to as hot-electron bolometers (HEBs). The electron heating rate under irradiation is high owing to the fast photon–electron interaction, while the thermal relaxation is related to the electron–phonon interaction time. The NEP is determined by bolometer temperature fluctuations and for metallic bolometers is written out as

$$\mathrm{NEP} = (4kT^2 G_{e-ph})^{0.5} = \left(4kT^2 \frac{C_e}{\tau_{e-ph}}\right)^{0.5} = \left(\frac{4kT^3 \gamma V}{\tau_{e-ph}}\right)^{0.5},$$

where G_{e-ph} is the effective heat conductivity for the heat transfer between electrons and phonons, C_e is the electron heat capacity, τ_{e-ph} is the electron–phonon interaction time, γ is the Sommerfeld constant in the expression for the electron heat capacity ($C_e = \gamma TV$), and V is volume of the sensitive element.

Karasik et al. [9] described an HEB with a titanium sensitive element having a volume of 3×10^{-3} μm^3 and niobium contacts, which was made on a silicon chip. At $T = 0.3$ K, the bolometer possessed a heat conductivity $G_{e-ph} = 4 \times 10^{-14}$ W K^{-1} and a NEP $= 3 \times 10^{-19}$ W $Hz^{-0.5}$.

For superconductor-based detectors, use is also made of structures with different ways of separating Cooper pairs. Among these detectors is one with a superconducting tunnel junction (STJ). Schoelkopf et al. [10] considered an $Al-AlO_x-Al$ structure, the so-called superconductor–insulator–superconductor (SIS) structure, which was kept at a temperature of 0.1 K together with an antenna of superconducting niobium. When a signal is read out by a one-electron transistor, the NEP may be lower than 1×10^{-19} W $Hz^{-0.5}$ under background-free conditions.

A nine-element set of detectors of an image camera intended for a submillimeter telescope was reported in Ref. [3]. Use was made of SIS-based detectors. The detector parameters were investigated at an effective background temperature of about 150 K. For a detector operating temperature of 0.3 K, the photocurrent was equal to 0.3 nA. The amplifier noise was close to the shot noise of the photocurrent, and the NEP was about 10^{-15} W $Hz^{-0.5}$. Raising the working temperature to 4 K resulted in an order-of-magnitude increase in the NEP. It was nevertheless lower than for a bolometer operating at the same temperature.

Using a camera mounted on the Atacama Submillimeter Telescope, the first astronomical observations of the Moon were performed for an atmosphere transmittance of about 1%.

Otani et al. [11] reported the fabrication of a five-element STJ detector with an Nb–Al–AlO_x–Al–Nb structure. The leakage current density at $T = 0.3$ K was equal to 1.5 pA μm^{-2}, the noise current at a frequency of 110 kHz was equal to 9×10^{-15} A $Hz^{-0.5}$, and the noise equivalent power was equal to 1.9×10^{-16} W $Hz^{-0.5}$ at a working temperature of 0.3 K. The peak of element sensitivity lay within the frequency range of 0.42–0.66 THz. The sensitivity of single-element heterodyne SIS detectors in the frequency range from 0.3 to 0.7 THz is limited by the noise of the microwave background and decreases at frequencies ranging 1.0–1.3 THz. H-W Hubers published a review [12] and outlined data on the frequency dependences of the double-band noise temperature for Schottky diodes, HEBs, and SIS detectors.

Huang et al. [13] reported the development of a detector for a portable submillimeter telescope operating at a frequency of 500 GHz. The 4.2-K working temperature of SIS detectors was provided by a two-stage cooling device 42 kg in weight and 0.06 m^3 in volume, which consumed a power of less than 1.2 kW for a maximum thermal load of 0.1 W in the working area. This telescope was employed to survey the Orion A celestial object. Divin et al. [14] reported the recording of terahertz signals in the vicinity of 0.5 THz using superconducting NbN–AlN–NbN junctions. The detection was made using Josephson junctions based on the high-temperature $YBa_2Cu_3O_{7-x}$ superconductor. At working temperature $T = 30$ K, the NEP was equal to 5×10^{-15} W $Hz^{-0.5}$, which was worse than for deeply cooled detectors.

Gao et al. [15] investigated a similar superconducting hot-electron NbN bolometer mixer with a planar antenna and an additional antireflection coating. They achieved noise temperature levels of 695 K (at a frequency of 0.65 THz), 904 K (1.6 THz), 1026 K (2.5 THz), and 1386 K (3.1 THz). Without depositing the antireflection coating, the noise temperature was about 300 K higher.

Ortolania et al. [16] and Shen et al. [17] discussed terahertz STJ detectors. STJ structures approximately 2 μm in diameter were formed of 100-nm thick superconducting aluminum and a tunnel barrier of aluminum oxide. The STJ resided on a niobium film, which absorbs terahertz radiation. The film, in turn, was located on a sapphire substrate, which weakly absorbs the terahertz radiation. The niobium film is single-crystalline, and the detector NEP level expected under low-background illuminations amounted to about 10^{-18} W $Hz^{-0.5}$. This is sufficient, as correctly believed by the authors, for employing this detector in ground-based astronomical laboratories, including its use for high-speed imaging in the terahertz region. Figure 2 shows the dependence of the ampere–watt responsivity on the radiation frequency for two Ti–Au antenna types. At $T = 4.2$ K, the NEP was about 10^{-15} W $Hz^{-0.5}$.

The feasibility of designing STJ photodetector arrays is determined primarily by the complexity of the technological procedures for making the STJ detector itself. In view of the extremely small dimensions of STJ detectors proper (on the order of the square of a micrometer), the making of a large-format photodetector array on these principles seems problematic.

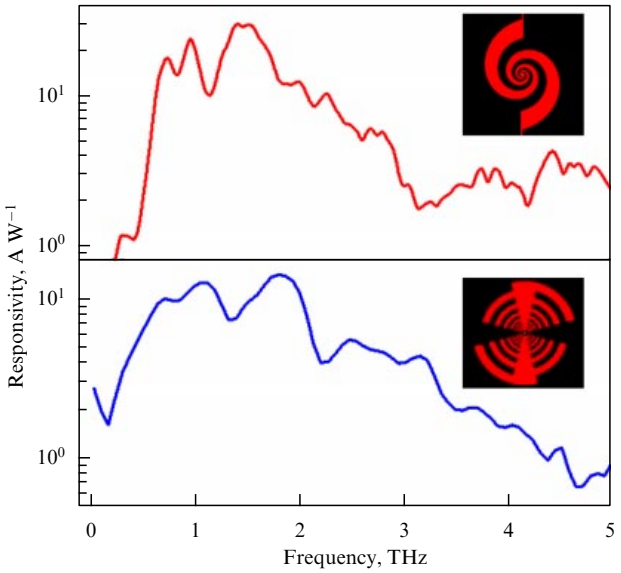

Figure 2. Ampere–watt responsivity of niobium microbolometers at $T = 4.2$ K.

Undoubtedly of interest are investigations into the feasibility of developing detectors that harness the effect of kinetic inductance. The inductance of superconducting strips depends on the concentration of Cooper pairs in the superconductor. Variations of inductance under irradiation may underlie the performance of high-sensitivity radiometers, bolometers, and mixers. Mazin et al. [18] emphasized not only the possibility of developing new superconducting detectors, but also the attendant method of signal readout from 10^4 detectors by only one high electron mobility transistor (HEMT) amplifier. However, the detector operating temperatures do not exceed one kelvin, which makes them unsuitable for industrial production, and no consideration was given to the problems of nonuniformity of the kinetic inductance of individual detectors, which may give rise to additional (geometric) noise.

3. Photon detectors

3.1 Extrinsic absorption photodetectors

To record far-IR radiation up to hundreds of micrometers, use is made of semiconducting extrinsic absorption photodetectors, commonly photoresistors (PRs), in which the absorbed radiation excites charge carriers localized on impurity levels. As a rule, the impurity absorption coefficient is 2–3 orders of magnitude lower than the absorption coefficient for valence–conduction band transitions. The operation of such a photodetector requires a specific temperature, depending on what wavelength the impurity absorption corresponds to — longer critical absorption wavelengths necessitate lower working temperatures. It is also pertinent to note that the limiting PR detectivity is $\sqrt{2}$ times lower than that of a photodiode with the same sensitivity edge.

For an extrinsic absorption PR material, use is made of germanium and silicon, germanium being tapped for making longer-wavelength PRs. The detectivity of these PRs is not infrequently limited by the background radiation fluctuations. However, this limitation takes effect at different

working temperatures, depending on the sensitivity critical wavelength.

Table 1 lists the characteristics of some Si-based IR PDs up to the 28–31 μm wavelength range, and some Ge-based PDs for the 29–193 μm range [19]. The second column of Table 1 gives the impurity ionization energy, while the third column shows the red sensitivity limit λ_{LW} and the PD working temperature, respectively. Furthermore, collected in Table 1 are the parameters of linear blocked-impurity-band (BIB) silicon structures and bilinear photodetectors based on PbSnTe:In solid solutions.

The quantum efficiency of a PR depends on the type and concentration of impurity, the radiation wavelength, and — which is significant — the thickness of the active layer, in which radiation absorption occurs. At the maximum of spectral responsivity, the quantum efficiency lies between 10 and 50%.

Under low-background conditions, for instance, on board a spacecraft, use is made of silicon- and germanium-based extrinsic PRs. Our attention is engaged by the PR working temperature which lies in the 2–5 K range. Table 1 contains the parameters of a stressed Ge:Ga PD, borrowed from Ref. [19]. In a stress-free state, the cutoff wavelength determined at half the peak responsivity is 114 μm. Data on the spectral dependence of the responsivity of zinc-, beryllium-, and gallium-doped germanium detectors are given by Leotin [20] and shown in Fig. 3. As is evident from the graphs, it is possible to shift the responsivity cutoff from approximately 25 to 200 μm by doping germanium with different impurities. On application of uniaxial pressure, the spectral responsivity curve shifts to a longer wavelength, and the cutoff wavelength at half the peak responsivity approaches 200 μm.

Kamiya et al. [21] reported the fabrication of a monolithic linear Ge:Ga detector array. A 3×20-pixel matrix has already been created, and work is underway to make a 64×64-pixel matrix. Figure 4 illustrates the structure of the prototype of a 5×5-pixel matrix.

The main problem with utilizing extrinsic PRs in the development of linear or matrix PD arrays is their low absorption coefficient, with the consequence that the PR must be sufficiently thick, up to a centimeter, to provide a high quantum efficiency. One way to solve the problem of PDAs for this spectral range is to use blocked-impurity-band structures as sensitive elements. For example, Esaev et al. [22] described the results of development of a linear BIB-structure-based PDA with a 1×64 format. The investigated linear PDAs exhibited a NEP value of about 10^{-16} W Hz$^{-0.5}$ at a working temperature of 10 K. The responsivity long-wavelength cutoff resided at 20–28 μm.

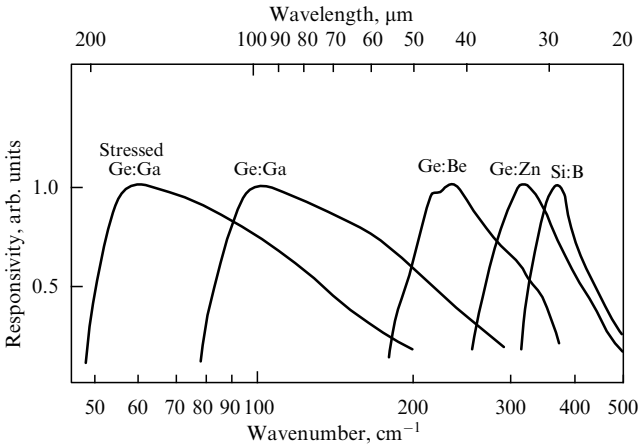

Figure 3. Spectral dependence of the relative responsivity of PDs based on doped germanium and silicon. Operating temperature is $T = 2$ K. (Borrowed from Ref. [20].)

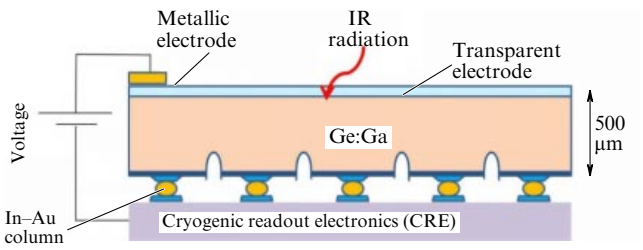

Figure 4. Schematic representation of a monolithic 5×5-pixel matrix.

3.2 Photodetectors with intrinsic absorption based on the films of indium-doped PbSnTe solid solutions

This section contains data on photon PDs utilizing intrinsic absorption in a narrow-band semiconductor lead–tin–tellurium solid solution doped with indium (PbSnTe:In). Unlike the majority of semiconductors, the band gap E_g in PbSnTe becomes narrower with decreasing temperature and even becomes zero for a certain content of tin and the composition-dependent temperature. In principle, this signifies that it is possible to obtain an extremely narrow band gap by varying the composition of PbSnTe:In and thereby provide efficient detection of far-IR radiation exploiting interband optical transitions.

3.2.1 Properties of PbSnTe:In and far-IR photodetectors. In 1979, Akimov et al. [23] and Vul et al. [24] discovered highly unusual properties in single-crystalline bulk samples of indium-doped PbSnTe:In solid solutions. The most important of these properties are the following:

Table 1. Characteristics of detectors sensitive in the region of $\lambda = 28 - 200$ μm

	Detector	ΔE, meV	λ_{LW}, μm (T, K)	NEP, W Hz$^{-0.5}$	PD format	Reference
1	Si:P (PR)	45.59	28 (5)	7.5×10^{-17}		[19]
2	Si:Sb (PR)	42.74	31 (5)	5.6×10^{-17}		[19]
3	Ge:Cu (PR)	43.21	29.5 (4.2)	1.0×10^{-15}		[19]
4	Ge:Ga (PR)	11.32	114 (3)	2.4×10^{-17}		[19]
5	Ge:Ga[1] (PR)	≈ 6	193 (2)	5.7×10^{-17}		[19]
6	Si:As (BIB)[2]		28 (7)	0.7×10^{-16}	64×1	[22]
7	PbSnTe:In	60	21 – 25 (7)	$\approx 10^{-18}$	128×2	[28]

[1] Stressed Ge.
[2] BIB structures.

— Fermi level stabilization in the forbidden band for a specific composition ($x \approx 0.22-0.28$) and a low dark conductivity for temperatures $T \leqslant 20$ K,

— high responsivity: a response to extremely weak radiation, including the radiation of bodies heated to a temperature only slightly higher than the temperature of the samples,

— long-term photosignal relaxation and residual conduction after cessation of illumination,

— photocurrent 'quenching' on application of a high electric field pulse.

The discovery of a high photosensitivity in the far-IR domain lent impetus to applied research aimed at developing IR PbSnTe:In-based PDs. Vasil'eva et al. [25] reported data concerning the growth and doping of PbSnTe:In films produced by molecular beam epitaxy (MBE) method on insulating BaF_2 substrates. The films were doped with indium in two ways: directly in the course of MBE, and during homogenizations in the vapor of a PbSnTe charge of requisite composition and indium telluride. The film properties after a series of diffusion annealings are shown in Fig. 5.

The resultant film parameters permitted conducting research on the development of multielement IR radiation detectors intended for the IKON project (''Infrared sky survey with a wide-angle cooled telescope aboard the NIKA Earth satellite in a solar-synchronous orbit'' [26]) carried out by the Space Research Institute, RAS. A multielement hybrid PDA for a 5–20-μm spectral range was described by Feofanov et al. [27] and Klimov and Shumsky [28]. It comprised a twin linear photodetector array, silicon circuits for photosignal processing (multiplexors) with control electronics, and connecting tails. A 64-element linear PD module was adopted as a basic PDA element.

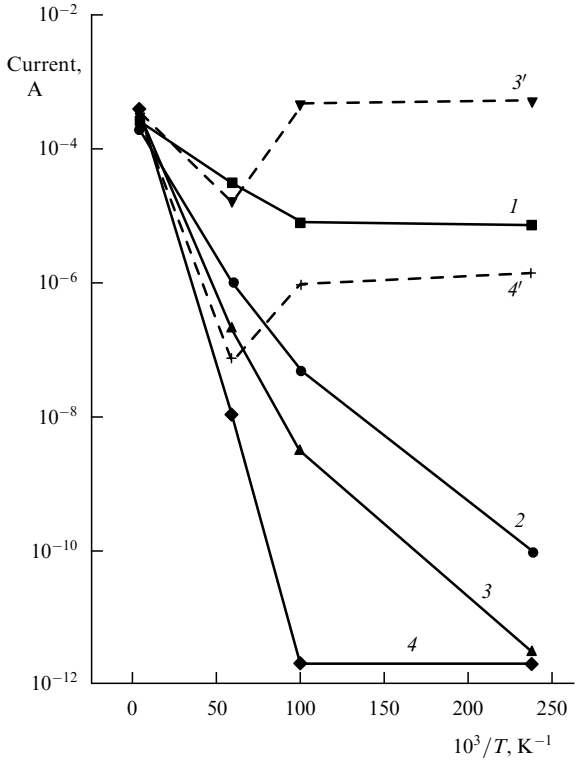

Figure 5. Current as a function of reciprocal temperature under successive annealing of an undoped PbSnTe film with a tin content of 26% in the presence of $[(Pb_{0.74}Sn_{0.26})_{1-x}In_x]_{1-y}Te_y$ ($x = 0.03$, $y = 0.5$) at a temperature of 460 °C. The total annealing time is 180 (*1*), 390 (*2*), 570 (*3*), and 770 (*4*) min. Curves *3′* and *4′* stand for the current under sample illumination. (Borrowed from Ref. [25].)

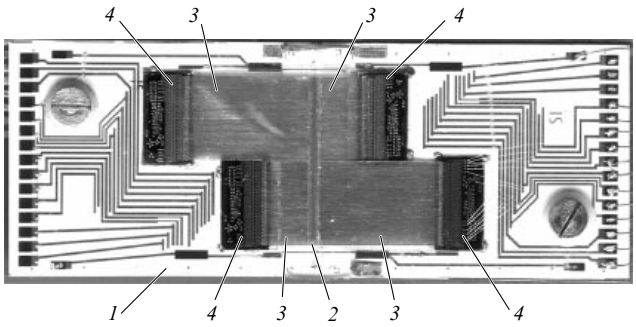

Figure 6. Linear phodetector device with a 2×128 element format: *1* – glassceramic substrate, *2* – 2×128 element PD, *3* – connecting tails, and *4* — silicon multiplexers with 64 inputs each. (Borrowed from Ref. [28].)

Figure 6 displays a photograph of a two-row linear PDA consisting of 2×128 photodetector elements, four silicon multiplexors with 64 inputs each, and four connecting tails based on polyimide film (the control electronics are not shown). The multiplexers on the right and on the left of the PD are spaced from each other for ease of attachment of the polyimide tails to them. In this case, the gaps between the neighboring elements at the center of the linear PD device, where the tails are attached, were the same as in the other parts.

The 64-element length of the basic PDA segment ensured a relative simplicity and a high percentage of the production yield of serviceable multiplexers. In this case, the modularity underlay the possibility of designing circuits for signal readout from both linear and relatively large-format matrix PDAs, intended for the solution of several practical problems. The low dark currents (below 10^{-11} A) of the individual elements of a set of PDs made it possible to apply the technology of silicon multiplexers operating at temperatures down to the liquid-helium temperature with a signal accumulation time of 0.001 s (a sampling frequency of 1 kHz). The gap was equal to 20 μm both between the linear PD array elements and between the two linear PD rows. The elements were illuminated from the side of epitaxial PbSnTe:In film.

Figure 7a plots the spectral dependence of the helium-temperature responsivity measured in a vacuum optical cryostat with the use of a cooled 1-mm thick cut-off $Pb_{0.79}Sn_{0.21}Te$ filter to reduce the background light. The sensitivity of the linear PD array extended to 20–22 μm.

The PDA threshold characteristics were measured on a cold test bench in a working temperature interval of 4–16 K. The responsivity of PDA elements depends on the radiator temperature. The photodetector integral ampere–watt responsivity reduced to the multiplexer input is plotted in Figure 7b in relation to the blackbody (BB) temperature.

Measurements of the noise of individual input multiplexer cells at helium temperature yielded a noise current $I_n \leqslant 2 \times 10^{-14}$ A Hz$^{-0.5}$. Therefore, the highest value of current responsivity, $S_{max} = 2 \times 10^5$ A W^{-1} approximately, and the intrinsic multiplexer noise yield a value of NEP $\approx 1 \times 10^{-19}$ W Hz$^{-0.5}$ or lower. In reality, this quantity was somewhat higher in different elements of the linear PDA device, depending on the working temperature and illumination level. This is due to the existence of intrinsic noise created by the photodetector elements, the nonlinearity of their

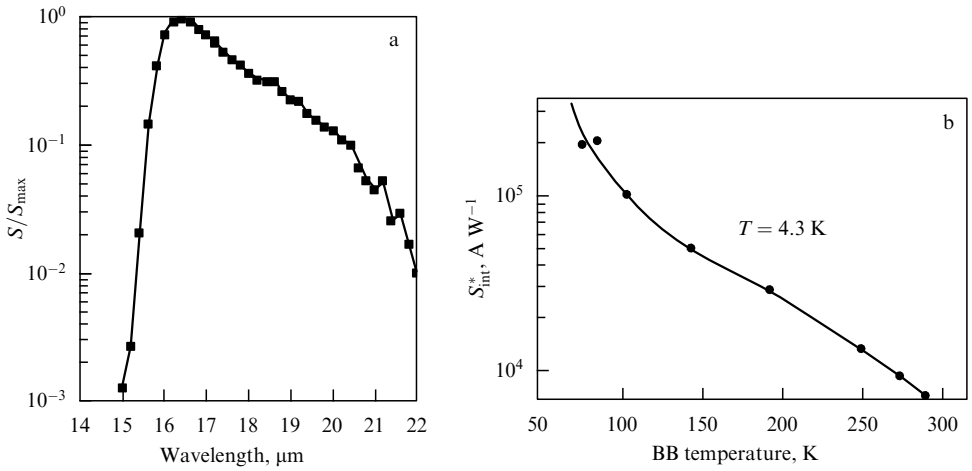

Figure 7. (a) Spectral dependence of the relative ampere–watt responsivity of the element of a linear PDA device, and (b) dependence of the integral ampere–watt responsivity on BB temperature. The dependences were taken for a PDA element bias $U = 2.2$ V for all BB temperatures. (Borrowed from Ref. [28].)

responsivity, and the temperature dependence of both of these parameters.

Figure 8 presents experimental data on the NEP of one of the fragments of a linear PDA device being part of a silicon multiplexer and of a linear 64-element PD array at a working temperature of 7 K. Plotted on the ordinate axis is the fraction of elements whose NEP is below the figure marked on the abscissa. One can see that approximately 85% of the elements of the fragment of the PDA device exhibit a NEP of less than 10^{-18} W Hz$^{-0.5}$. Figure 8 also suggests that the attained parameters are not limiting for PbSnTe:In-based PDs, since the individual elements of the linear PDA device at $T = 7$ K exhibit a NEP below 5×10^{-19} W Hz$^{-0.5}$.

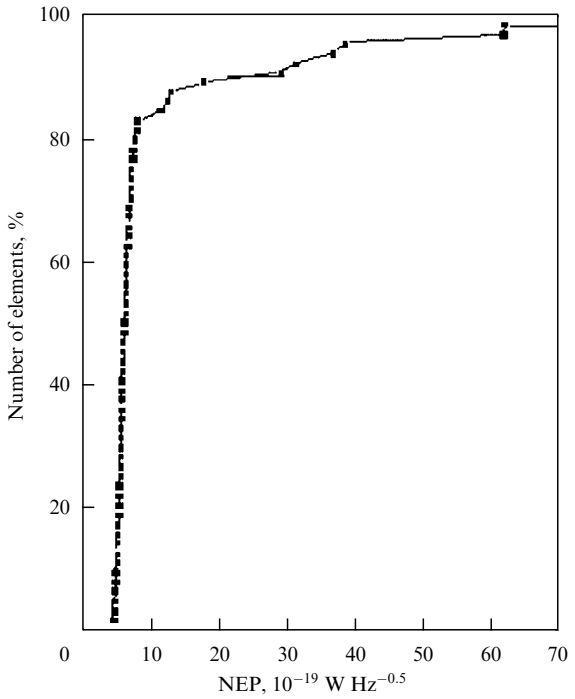

Figure 8. Distribution over noise-equivalent-power of the number of elements for a linear PDA device fragment. The PDA working temperature is 7 K, and the radiator cavity temperature $T_{BB} = 78$ K. (Borrowed from Ref. [28].)

Since the photosensitive surface area of the linear PDA element was $A = 10^{-4}$ cm^2, the NEP $= 10^{-18}$ W Hz$^{-0.5}$ corresponded to the detectivity $D^* = 10^{16}$ cm Hz$^{0.5}$ W^{-1}, which is realized in this spectral region only under low background illumination.

The linear PDA device technology described above has the potential both for lowering the NEP and for improving the uniformity of response of the elements by employing initial barium fluoride substrates of higher uniformity or replacing them, for instance, with silicon, as well as by improving the uniformity of the characteristics of input multiplexer cells.

Some limitations on using the linear PDA device developed may arise primarily from its rather long response time, especially at low illumination levels. At the same time, these limitations are not a matter of principle. It is well known that the photoconductivity in PbSnTe:In may be 'quenched' in different ways, one being to apply to photosensitive elements for a short time a sufficiently strong electric field corresponding (for a size of the photosensitive area on the order of 100 μm) to a voltage of about 20 eV. In this case, the problem of shortening the PDA response time may be solved by a minor design modification of multiplexers and their control unit.

Furthermore, requirements on the response time of individual elements are, as a rule, relaxed for PDA devices with a large number of elements. In particular, in a large-format matrix PD device, requirements on the speed of response are determined by the frame-repetition frequency, which typically ranges between tenths of a frame per second and tens of frames per second. The prospects for application of the above PDA devices, including operation at an elevated working temperature, are discussed by Klimov et al. [29].

Akimov et al. [30] described the development of technological elements for a PDA device based on $Si-CaF_2-BaF_2-PbSnTe:In$ multilayer structures, in which both PDs and preliminary signal processing circuits may be accommodated on a silicon substrate. PDs with a 288×2-element format have been made (with element dimensions of 25×25 μm, the linear arrays are horizontally shifted relative to each other by 25 μm). The parameters of 18 individual PD elements were selectively measured. Measurements were made at a bias voltage $U = 0.06$ V on photosensitive areas and a radiator temperature $T_{BB} = 293$ K.

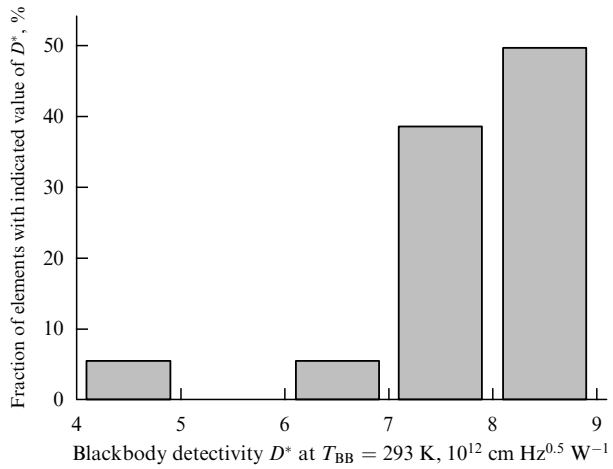

Figure 9. Detectivity distribution histogram of the elements of a linear PDA device at a working temperature of 21.2 K. (Borrowed from Ref. [30].)

Figure 9 displays a detectivity histogram of the elements of a linear PD at a working temperature $T = 21.2$ K. In this case, with the exception of two elements whose parameters deviate significantly from the average ones, the spread in responsivity and dark resistance amounts to about $\pm 15\%$ for the 18 areas investigated. The high uniformity of parameters is due to the higher uniformity of the $Si-CaF_2-BaF_2$ structure used as the substrate than with substrates of single-crystalline barium fluoride.

One can see that the detectivity of about 90% of the measured elements for the linear PD ranges from 7.2×10^{12} to 8.7×10^{12} cm Hz$^{0.5}$ W^{-1}. A comparison of the PD parameters made on $Si-CaF_2-BaF_2-PbSnTe:In$ structures with the parameters of the elements of a hybrid PDA device with multiplexers [28] based on PbSnTe:In films, which were grown by the same method on single-crystalline BaF_2, offers the following conclusions. In the former case, the NEP $\approx 3 \times 10^{-16}$ W Hz$^{-0.5}$ or lower for 90% of the elements at a working temperature of 21.2 K; in the latter case, the NEP $\approx 8 \times 10^{-17}$ W Hz$^{-0.5}$ or lower for 90% of the elements at a significantly lower working temperature $T = 15$ K.

Variations of PbSnTe conductivity under far-IR and SMM irradiation have been observed in several studies, for instance, by Belogorokhov et al. [31] and Khokhlov et al. [32]. The photoconductivity of PbTe:Ga was discovered in the frequency range of 100–460 cm^{-1} ($\lambda = 21.7-100$ μm) [31]. The authors of Ref. [32] discovered the photoconductivity of PbSnTe:In at wavelengths of 90 and 116 μm, which was measured employing BB radiation and a set of optical filters. The responsivity of this material in the terahertz spectral region was also reported in Refs [33–40].

Akimov et al. [35] hypothesized that there are several energy levels in the forbidden band of PbSnTe:In, located several millielectron-volts from the bottom of the conduction band, which are electron-trapping sites. When occupied by electrons, they may be responsible for nonequilibrium conduction under terahertz irradiation.

Klimov et al. [36] reported the responsivity of PbSnTe:In to BB radiation with a temperature ranging from 60 to 20 K. An analysis of the dependence of the photosignal on the BB temperature combined with the use of a cutoff cold optical filter permitted estimating the responsivity range, which corresponds to wavelengths ranging 300–400 μm. Responsivity studies of the same samples made with an HCN laser, which radiated at a wavelength of 336.8 μm [36–39], revealed that the current increased under illumination of the sample in this case, the absolute value of the current increment increasing with the voltage applied to the structure.

An analysis of results suggests the existence of two possible mechanisms of occurrence of a photosignal under terahertz irradiation. In the first case, the absorption of SMM radiation causes a temperature shift of a ferroelectric phase transition, which corresponds to an increase in static permittivity ε. At helium temperatures, under conditions of limitation of current in PbSnTe:In by a spatial charge, the increase in ε under SMM irradiation will lead to enhancement of the current.

More likely is the second mechanism, whereby the photosignal is induced by SMM radiation due to localized electron transitions to the conduction band from levels located in the forbidden band. One would expect a manifestation of PbSnTe:In photosensitivity in the terahertz region up to wavelengths of several hundred micrometers, depending on the energy (or spectrum) of these levels.

Klimov and Shumsky [41] calculated the photocurrent in PbSnTe:In in the terahertz region at $T = 4.2$ K. The calculation made use of the energy spectrum of the electron-trapping sites in the forbidden band derived from an analysis of volt–ampere characteristics in the space-charge-limited current (SCLC) mode. The calculated values of the SMM photosignal, which were determined by evaluating the population of the corresponding levels in the SCLC mode and calculated as functions of the voltage across the structure (Fig. 10), were compared with the experimental dependences for two wavelengths of free-electron laser (FEL) radiation, 130 and 198 μm, which corresponds to trap ionization energies of 9.5 and 6.2 meV.

Figure 10 suggests that the calculation and experiment are in satisfactory agreement for $\lambda = 130$ μm (curve *1*), while the agreement for $\lambda = 198$ μm is satisfactory only in the low-voltage region (curve *2*). However, observed in both cases is a rise in current with increasing voltage, which leads to higher occupation numbers for the electron-trapping sites due to an increase in injection level from the contacts, as follows from

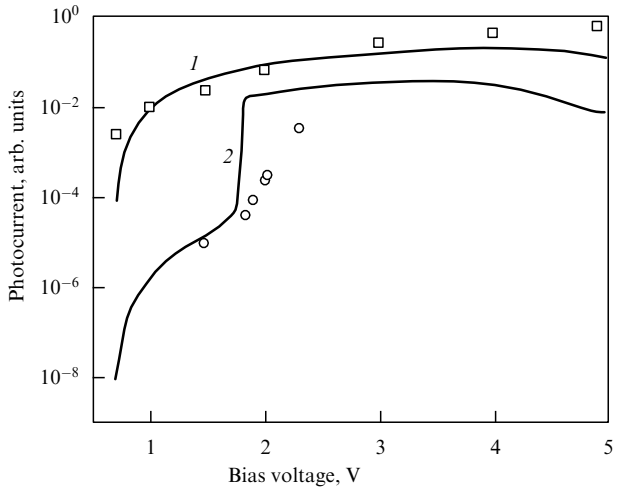

Figure 10. Experimental (squares and circles) and calculated dependences of the current on the bias voltage under FEL irradiation at wavelengths of 130 μm (squares, curve *1*) and 198 μm (circles, curve *2*).

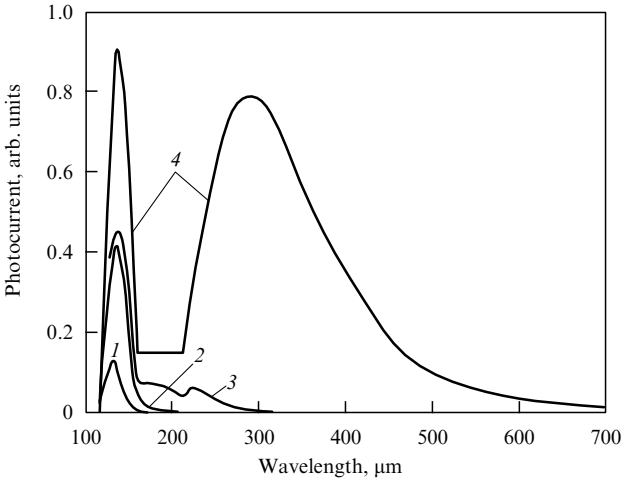

Figure 11. Calculated spectral characteristics of the PbSnTe:In structure in the SCLC mode; $U = 1.16$ (*1*), 1.79 (*2*), 1.83 (*3*), and 2.95 (*4*) V.

the SCLC theory. In the view of the authors, the possible disagreement between theory and experiment may be caused by following circumstance: in reality, the energy distribution of the trapping sites is quasicontinuous and not discrete (two-level), as was assumed in simplified calculations.

An investigation into the appearance of PbSnTe:In sensitivity in the terahertz radiation range was continued in Ref. [42]. The authors noted that a distinguishing feature of photocurrent in the SCLC mode is its strong dependence on the local level population which, in turn, depends on the magnitude of electron injection, i.e., on the applied voltage. The further this level is spaced from the equilibrium Fermi level, the more strongly this dependence has to manifest itself.

The spectral dependences of the structure sensitivity in the terahertz radiation range were calculated for the same parameters of the sites as in Ref. [41]. The simulated data are given in Fig. 11. One can see that raising the injection level (increasing the voltage) leads to increasing the photocurrent throughout the entire spectral range, but this growth is most pronounced for $\lambda > 200$ μm. This is due to the fact that as the voltage increases, the injection current also increases and electron filling of the sites located progressively closer to the bottom of the conduction band occurs. Consequently, electron transitions to the conduction band from shallower sites become possible, and just these sites are excited by SMM radiation of progressively longer wavelength. Simultaneously, the photocurrent strength at shorter wavelengths changes only slightly under a large increase in voltage, because these levels are filled with electrons even for a relatively low applied voltage. Therefore, a detector reliant on SMM-radiation-induced transitions from the trapping sites in PbSnTe:In to the allowed band can operate in the applied-voltage-dependent spectral responsivity mode.

By and large, the existence of levels of localized states in the forbidden band and the electron injection from contacts account for the shape of the volt–ampere characteristic, the long-term photoresponse, the quenching of photocurrent by a pulse generated in a strong electric field, and the sensitivity to SMM radiation. Akimov et al. [43] presented the results of investigations into sensitivity to terahertz radiation for $Pb_{1-x}Sn_xTe:In$ structures with an elevated tin content (over 30%). At $T = 4.2$ K and a tin content $x = 0.25$, the PbSnTe:In band gap E_g is close to 60 meV (the long-wavelength cutoff λ_{LW} of intrinsic absorption is near 20 μm), while $E_g = 0$ at $x = 0.35$. In the domain of intermediate tin content, E_g decreases and λ_{LW} increases. The possibility of obtaining a high-resistance state without illumination at helium temperatures remained unexplored for these compositions. The authors of Ref. [44] succeeded in obtaining this state and reported the data for PbSnTe:In samples with $x = 0.32$ ($\lambda_{LW} \approx 70$ μm).

Figure 12 depicts the time characteristics of the photocurrent in PbSnTe:In samples exposed to FEL radiation at 141- and 205-μm wavelengths. One can see that increasing the voltage leads to an increase in current under irradiation (Fig. 12b). An estimate of the threshold sensitivity of detectors based on such structures yielded an NEP better than at least 5×10^{-9} W Hz$^{-0.5}$.

The parameters of PDs fabricated on the basis of $Pb_{1-x}Sn_xTe:In$ films with $x = 0.32$ and prospects of their application are reported in Ref. [44]. Noise measurements were made with a selective voltage amplifier at a frequency of 1025 Hz and a load resistance $R_{RL} = 4.45$ kΩ. The width of the amplifier noise band was $\Delta f = 20.5$ Hz. The root-mean-square noise of the sample was calculated as the difference between the squares of noise voltages at the bias voltage $U = 0.14$ V and $U = 0$. The mean value of a noise current was equal to 1.9×10^{-13} A. The detector parameters were measured using a BB radiation whose temperature could be varied over a sufficiently wide range.

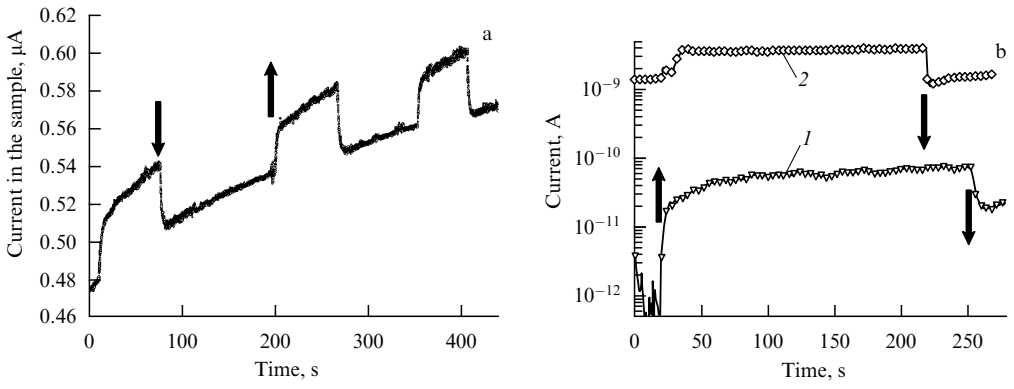

Figure 12. Time dependence of a current flowing through a sample with $x = 0.32$ and exposed to FEL radiation of wavelengths 141 μm (a) and 205 μm (b). The instants of onset and cessation of laser irradiation are indicated with arrows. The voltage across the structure is 0.025 V (*1*) and 0.82 V (*2*).

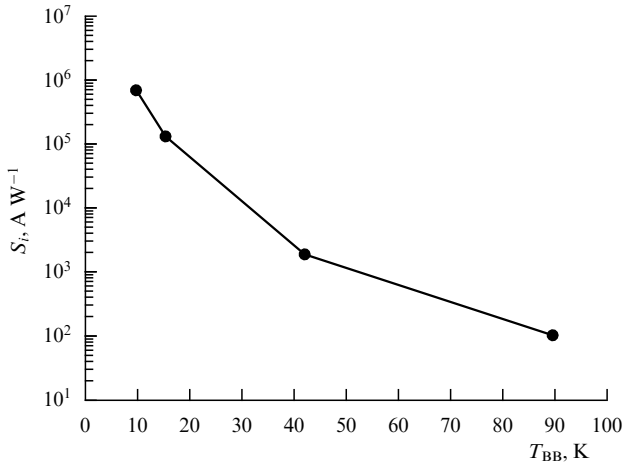

Figure 13. Dependence of the ampere–watt responsivity on the BB temperature for a sample of composition $x = 0.32$. The bias voltage across the sample is 0.14 V.

Table 2. Detectivity and NEP of a $Pb_{1-x}Sn_xTe$:In ($x = 0.32$)-based PD.

BB temperature, K	D^*, cm Hz$^{1/2}$ W^{-1}	NEP, W Hz$^{-1/2}$
15	8.2×10^{16}	3.1×10^{-19}
42	1.2×10^{15}	2.1×10^{-17}
90	6.4×10^{13}	4×10^{-16}

The ampere–watt PD responsivity was calculated for a stationary current strength. In this case, the incident radiation flux was defined by the formula

$$P = \frac{\pi d^2}{4} \frac{A}{\pi L^2} \sigma (T_1^4 - T_2^4),$$

where d is the diameter of the radiator output aperture stop, A is the dimension of the photosensitive area, L is the distance between the aperture stop and the photosensitive area, T_1 is the radiator temperature, and T_2 is the PD temperature. Figure 13 shows the dependence of the ampere–watt responsivity on the BB temperature.

Table 2 lists the values of detectivity D^* and the NEP calculated proceeding from the measured values of ampere–watt responsivity noise level.

An important experimental result concerns the emergence of photocurrent at low (down to 10 K) BB temperatures, which cannot be attributed to interband transitions due to the practically complete absence of photons with the corresponding energy. According to calculations, for $T_{BB} = 10$ K and samples of composition $x = 0.32$, the photon flux on the sample in the intrinsic absorption region is insufficient to account for the emergence of a photosignal due to electron–hole pair generation. Therefore, it may be assumed that the observation of photocurrent is due to the excitation of electrons occupying levels in the forbidden gap, whose level depths correspond to film sensitivities in the far-IR or terahertz spectral regions.

3.2.2 Detectors with an intermediate thermal shield. Data on the responsivity of far-IR and terahertz radiation detectors with direct radiation absorption by a PbSnTe:In-based photosensitive PD element were outlined in Section 3.2.1. In the development of SMM-range imaging systems, an alternative version involves the employment of an intermediate absorbing thermal shield to convert the SMM radiation to thermal radiation with its subsequent detection by an IR PD or a PDA device (see, for instance, Ref. [45]). The possibility of implementing this method with the use of detectors based on $Pb_{1-x}Sn_xTe$:In films was reported in Ref. [46].

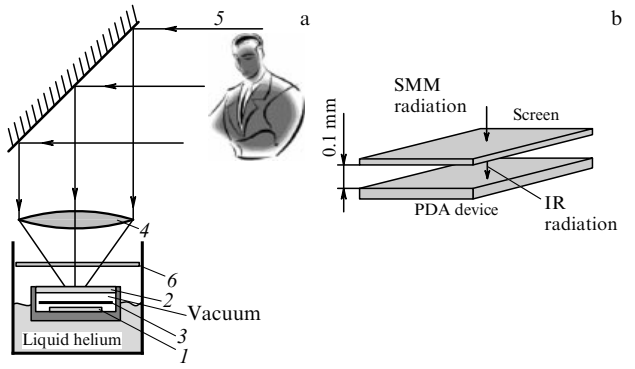

Figure 14. (a) Schematic diagram of a passive imaging system in the terahertz wavelength range with an intermediate thermal screen, and (b) arrangement of the screen and detector matrix.

Figure 14 represents a schematic diagram of a passive SMM imaging system, i.e., a system operating without terahertz backlighting, only on the strength of intrinsic thermal radiation of an object with a temperature close to room temperature. A matrix detector (*1*) is accommodated in a vacuum chamber, which is cooled to helium temperature and which has an input window with a cutoff filter (*2*). Placed in the immediate vicinity of the detector in a vacuum at $T = 30-80$ K is a thin thermal screen (*3*), on which an uncooled submillimeter lens (*4*) images the object (*5*) at close-to-room temperature.

The screen warms under the action of the SMM radiation from the object and the corresponding low-temperature thermal field is formed on the screen, whose radiation is incident on the far-IR matrix detector operating in low-background conditions. Actually, conversion occurs of the primary terahertz radiation spectrum to shorter-wavelength radiation. The capabilities of this system are determined by the sensitivity of the far-IR matrix PDA device to the thermal radiation emanating from the intermediate low-temperature screen.

Figure 15 shows the calculated dependence of the power radiated by an element of the screen surface 100×100 μm in size in the wavelength range from zero to λ_{LW} at a screen temperature T_s. Also shown here are the real NEP values for radiation detectors of the same size made of different materials, which may be placed in the immediate vicinity of the screen in this setup. One can see that this setup calls for a PD with the longest attainable sensitivity cutoff in order to analyze the temperature profile of a screen heated to a temperature of less than 80 K, which is realized in the imaging setup under consideration. The use of PbSnTe:In-based PDs permits recording screen temperatures below 40 K. Raising the Sn content will narrow the band gap in PbSnTe:In and make it possible to measure even lower screen temperatures.

Galkin et al. [47] described the properties of several components developed for an imaging system with a PbSnTe:In-based intermediate screen, including absorption

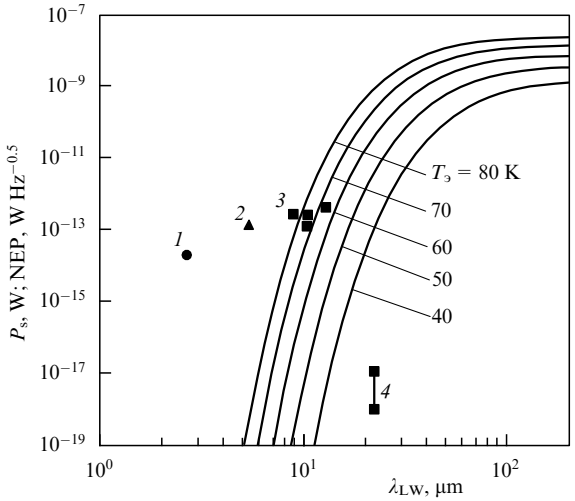

Figure 15. Power P_s radiated by an element of a screen in the wavelength range from zero to the long-wavelength PD sensitivity cutoff at a screen temperature T_s (solid curves) and NEP of different PDs with their real long-wavelength sensitivity cutoffs: InAs (*1*), InSb (*2*), CdHgTe (*3*), and PbSnTe:In (*4*).

coatings for the screen. Investigations were made of different metallic coatings (Au, Pd, Ni, InGaSn) several dozen nanometers in thickness, which were chemically deposited from solutions onto a thin polymer film. Significant absorption was observed only in nickel-based films, while thin films of other metals were either transparent in the terahertz region (Au, Pd) or possessed too-high a reflectivity (InGaSn). The spectral dependences of the transmittances and reflectivities of the absorptive coatings in the 45–350 cm^{-1} range are exemplified in Fig. 16.

The films whose spectral characteristics are depicted in Fig. 16 differed in metal deposition time (in thickness). The optical properties of highly reflective samples (Fig. 16a) were typical for thin metal films [48]. Both sample types were investigated with a scanning electron microscope. The weakly reflective samples obtained for short deposition times were found to consist of crystallites smaller than 5–10 nm in size. These samples were employed for making the screen. Calculations of the dependence of the signal-to-noise ratio on the screen temperature, as well as measurement data obtained on the pilot sample are indicative, in the authors' opinion, of the possibility, in principle, of employing this scheme to develop a terahertz imaging system [49].

4. Conclusion

This paper discusses only a small part of the work concerned with photodetector array devices for the far-IR and SMM spectral regions, including imaging systems. When estimating the prospects and areas of application of one PDA device or another in the operation in the passive mode, i.e., employing the intrinsic thermal radiation of the objects under observation, the following must be taken into account.

At the Earth surface level, terahertz radiation is strongly attenuated by the atmosphere. Specifically, it amounts to about 1–10 dB km^{-1} in the 100–500 GHz frequency range, while in the range of 500 GHz–1 THz the attenuation varies from 10 to 100 dB km^{-1} and over [50]. Due to this, as well as to a high background radiation flux, it is unlikely that the PDs considered in our work will enjoy wide use under terrestrial conditions. That is why the main areas of application of high-threshold PD and PDA devices for the IR and SMM spectral regions supposedly involve problems solved under low-background and extra-atmospheric conditions. This may be, for instance, the detection of weakly heated objects from their intrinsic thermal radiation beyond the terrestrial atmosphere against the background of a 'cold cosmos', including the recording of the radiation from astronomical objects.

Suitable for solving problems on radiation detection in the specified spectral regions are, in principle, PDA devices based on superconducting materials doped with silicon and germanium, or based on the films of a narrow-band PbSnTe:In solid solution. The advantages of matrix photodetectors based on PbSnTe:In films are a somewhat higher working temperature, a higher absorption coefficient in the intrinsic absorption band, and, most importantly, the practically developed PDA fabrication technology, including multiplexers. It is based on conventional semiconductor technologies, including silicon ones. The employment of thin PbSnTe:In films is possible owing to a high absorption coefficient in the domain of intrinsic absorption of this material, which is inaccessible for impurity semiconductor PDs of the submillimeter range.

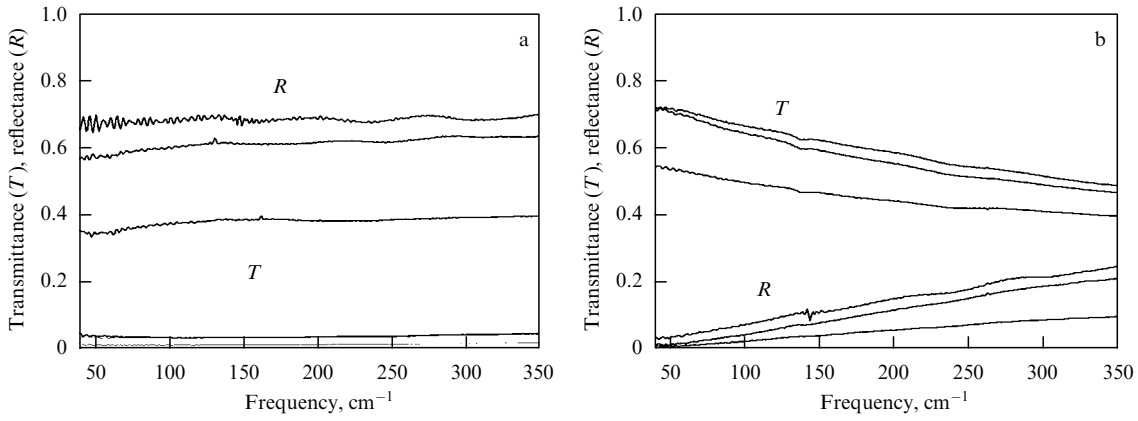

Figure 16. Spectral dependences of the transmission and reflection coefficients of highly reflective (a) and weakly reflective (b) samples with Ni coatings [47].

References

1. Ryabova L I, Khokhlov D R *Phys. Usp.* **57** 959 (2014); *Usp. Fiz. Nauk* **184** 1033 (2014)
2. Khokhlov D R *Phys. Usp.* **49** 955 (2006); *Usp. Fiz. Nauk* **176** 983 (2006)
3. Rogalsky A, Sizov F *Opto-Electron. Rev.* **19** 346 (2011)
4. Voitsekhovskii A V et al. *Nanoinzheneriya* (11) 7 (2012)
5. Simoens F et al., in *IRMMW-THz 2005. Proc. of the Joint 30th Intern. Conf. on Infrared and Millimeter Waves, 13th Intern. Conf. on Terahertz Electronics, Williamsburg, Virginia, USA, September 19 – 23, 2005* (Piscataway, N.J.: IEEE, 2005) p. 405
6. Pajot F et al. *J. Low Temp. Phys.* **151** 513 (2008)
7. Pajot F et al., in *Proc. of the Intern. Conf. on Infrared, Millimeter and Terahertz Waves, Busan, Korea, September 21 – 25, 2009* (Piscataway, N.J.: IEEE, 2009) p. 398
8. Bintley D et al., in *Proc. of the Intern. Conf. on Infrared, Millimeter and Terahertz Waves, Rome, Italy, September 5 – 10, 2010* (Piscataway, N.J.: IEEE, 2010) p. We-F3.1
9. Karasik B S et al. *IEEE Trans. Appl. Supercond.* **17** 293 (2007)
10. Schoelkopf R J et al. *IEEE Trans. Appl. Supercond.* **9** 2935 (1999)
11. Otani C et al. *Proc. SPIE* **5354** 86 (2004)
12. Hubers H-W *IEEE J. Select. Top. Quantum Electron.* **14** 378 (2008)
13. Huang S P et al., in *IRMMW-THz 2006*: *Conf. Digest of the 2006 Joint 31st Intern. Conf. on Infrared and Millimeter Waves and 14th Intern. Conf. on Terahertz Electronics, September 18 – 22, 2006, Shanghai, China* (Eds X C Shen et al.) (New York City, NY: IEEE, 2006) p. 178
14. Divin Y Y et al., in *IRMMW-THz 2006*: *Conf. Digest of the 2006 Joint 31st Intern. Conf. on Infrared and Millimeter Waves and 14th Intern. Conf. on Terahertz Electronics, September 18 – 22, 2006, Shanghai, China* (Eds X C Shen et al.) (New York City, NY: IEEE, 2006) p. 345
15. Gao J R et al., in *IRMMW-THz 2006*: *Conf. Digest of the 2006 Joint 31st Intern. Conf. on Infrared and Millimeter Waves and 14th Intern. Conf. on Terahertz Electronics, September 18 – 22, 2006, Shanghai, China* (Eds X C Shen et al.) (New York City, NY: IEEE, 2006) p. 545
16. Ortolania M et al., in *Proc. of the Intern. Conf. on Infrared, Millimeter and Terahertz Waves, Rome, Italy, Sept. 5 – 10, 2010*, Tu-A2.1
17. Shen X-F, Li J, Shi S-c, in *IRMMW-THz 2006*: *Conf. Digest of the 2006 Joint 31st Intern. Conf. on Infrared and Millimeter Waves and 14th Intern. Conf. on Terahertz Electronics, September 18 – 22, 2006, Shanghai, China* (Eds X C Shen et al.) (New York City, NY: IEEE, 2006) p. 344
18. Mazin B et al. *Proc. SPIE* **4849** 283 (2002)
19. Sclar N *Prog. Quantum Electron.* **9** 149 (1984)
20. Leotin J *Proc. SPIE* **666** 81 (1986)
21. Kamiya S et al., in *Proc. of the Intern. Conf. on Infrared, Millimeter and Terahertz Waves, Rome, Italy, September 5 – 10, 2010* (Piscataway, N.J.: IEEE, 2010) p. We-F3.6
22. Esaev D G, Sinitsa S P, Frantsuzov A A, in *Matrichnye Fotopriemnye Ustroistva Infrakrasnogo Diapazona* (Infrared Photodetector Arrays) (Exec. Ed. S P Sinitsa) (Novosibirsk: Nauka, 2001) p. 376
23. Akimov B A et al. *JETP Lett.* **29** 9 (1979); *Pis'ma Zh. Eksp. Teor. Fiz.* **29** 11 (1979)
24. Vul B M et al. *JETP Lett.* **29** 18 (1979); *Pis'ma Zh. Eksp. Teor. Fiz.* **29** 21 (1979)
25. Vasil'eva L F et al. *Inorganic Mater.* **37** 144 (2001); *Neorg. Mater.* **37** 193 (2001)
26. Sholomitskii G B et al. "Infrakrasnyi obzor neba s shirokougol'nym okhlazhdaemym teleskopom na solnechno-sinkhronnom ISZ 'Nika-I' (Proekt IKON)" ("Infrared sky survey with a wide-angle cooled telescope aboard a solar-synchronous orbit satellite 'Nika-I' (IKON Project)", Preprint No. 1919 (Moscow: IKI RAS, 1995)
27. Feofanov G N et al., in *Proc. of the Intern. Semiconductor Device Research Symp., ISDRS'95, Charlottesville, Virginia, USA, 5 – 8 December 1995* Vol. 1 (Piscataway, NJ: IEEE, 1995) p. 291
28. Klimov A E, Shumsky V N, in *Matrichnye Fotopriemnye Ustroistva Infrakrasnogo Diapazona* (Infrared Photodetector Arrays) (Exec. Ed. S P Sinitsa) (Novosibirsk: Nauka, 2001) p. 308
29. Klimov A E et al. *Nauka Tekhnol. Promyshlennosti* **4** (1) 97 (2006)
30. Akimov A N et al. *Tech. Phys. Lett.* **35** 524 (2009); *Pis'ma Zh. Tekh. Fiz.* **35** (11) 88 (2009)
31. Belogorokhov A I et al. *JETP Lett.* **63** 353 (1996); *Pis'ma Zh. Eksp. Teor. Fiz.* **63** 342 (1996)
32. Khokhlov D R et al. *Appl. Phys. Lett.* **76** 2835 (2000)
33. Klimov A E, Shumsky V N *Proc. SPIE* **5964** 95 (2005)
34. Klimov A E, Kubarev V V, Shumsky V N, in *Proc. of the 8th Russia-CIS-Baltic-Japan Symp. on Ferroelectricity, Tsukuba, Japan, May 15 – 19, 2006, Abstract Book*, p. 63
35. Akimov A N et al. *Semiconductors* **40** 164 (2006); *Fiz. Tekh. Poluprovod.* **40** 169 (2006)
36. Klimov A E, Kubarev V V, Shumsky V N *Ferroelectrics* **347** 111 (2007)
37. Akimov A N et al. *Priklad. Fiz.* (6) 12 (2007)
38. Akimov A N et al. *J. Surf. Investigat. X-Ray Synchr. Neutron Tech.* **1** (6) 711 (2007); *Poverkhnost Rentgen. Sinkhrotron. Neitron. Issled.* (12) 18 (2007)
39. Shumskii V N *Elektronika Sibiri* (3) 147 (2008)
40. Klimov A E, Shumsky V N, in *Proc. of the Intern. Conf. on Infrared, Millimeter and Terahertz Waves, Busan, Korea, September 21 – 25, 2009* (Piscataway, N.J.: IEEE, 2009) p. 316
41. Klimov A E, Shumsky V N *Physica B* **404** 5028 (2009)
42. Klimov A E, Shumsky V N, in *Ferroelectric-Physical Effects* (Ed. M Lallart) (Rijeca: InTech, 2011) p. 527
43. Akimov A N et al. *Optoelectron. Instrum. Data Proces.* **49** 492 (2013); *Avtometriya* **49** (5) 86 (2013)
44. Akimov A N et al. *Russ. Microelectron.* **42** (2) 59 (2013); *Mikroelektronika* **42** (2) 83 (2013)
45. Cherkassky V S et al. *Nucl. Instrum. Meth. Phys. Res. A* **543** 102 (2005)
46. Akimov A N et al. *Optoelectron. Instrum. Data Proces.* **43** 342 (2007); *Avtometriya* **43** (4) 63 (2007)
47. Galkin P S et al. *Optoelectron. Instrum. Data Proces.* **45** 353 (2009); *Avtometriya* **45** (4) 85 (2009)
48. Abeles F, in *Physics of Thin Films* Vol. 6 (Eds M H Francombe, R W Hoffman) (New York: Academic Press, 1971) p. 151
49. Klimov A E, Shumsky V N, Patent RF No. 2399990 of 23.09.2009 (2010)
50. Korotaev V V et al. *Osnovy Teplovideniya* (Foundations of Thermal Imaging) (St. Petersburg: NIU ITMO, 2012)